





Analysis of a Mechanism Used to Operate an Oscillating Separator

Emilian Mosnegutu ¹, Luminița Bibire ¹, Dana Chitimuș ^{1,*}, Mirela Panainte-Lehăduș ^{1,*}, Marcin Jasiński ², Grzegorz Przydatek ³ and Nicoleta Sporea ⁴

¹ Faculty of Engineering, “Vasile Alecsandri” University of Bacău, 600115 Bacău, Romania; emos@ub.ro (E.M.); lbibire@ub.ro (L.B.)

² Institute of Vehicles and Construction Machinery Engineering, Warsaw University of Technology, 02-524 Warsaw, Poland; marcin.jasinski@pw.edu.pl

³ Faculty of Engineering Science, University of Applied Sciences in Nowy Sacz, 33-300 Nowy Sacz, Poland; gprzydatek@ans-ns.edu.pl

⁴ Faculty of Mechanical Engineering and Mechatronics, University Politehnica of Bucharest, 060042 Bucharest, Romania; nicoleta.sporea@upb.ro

* Correspondence: dana.chitimus@ub.ro (D.C.); mirelap@ub.ro (M.P.-L.)

Abstract: This article presents a comparative study of two different kinds of processes that produce oscillatory motion on a work surface during the mechanical separation process. The investigation began with determining the trajectory produced by the oscillating separator’s active component of the classical drive mechanism. Based on this, a second mechanism—the six-bar mechanism—was created using the WATT program, and a mathematical analysis was conducted. The comparative examination of the two mechanisms was carried out using OriginPro, Mathcad, and Roberts software. This study’s findings all point to the same conclusion: the newly developed mechanism produces the same trajectory as the classical mechanism when viewed through the lens of the reference element, or the element that causes the oscillatory movement. However, when looking at the operating parameters, there was a noticeable difference in the movement’s speed and the angle of the crank when producing its maximum speed. Theoretically, this new mechanism increases the speed at which solid particles move across a work surface. However, this difference cannot be characterized as positive or negative because further research is required to determine how the nature of solid particles and the work surface’s inclination affect this process, in addition to this mechanism. The identification of the mathematical equations of motion for the constituent parts of the mechanism under study is the novelty produced of this paper.

Keywords: oscillatory motion; six-bar mechanism; geometric coordinates



check for
updates

Citation: Mosnegutu, E.; Bibire, L.; Chitimuș, D.; Panainte-Lehăduș, M.; Jasiński, M.; Przydatek, G.; Sporea, N. Analysis of a Mechanism Used to Operate an Oscillating Separator. *Appl. Sci.* **2024**, *14*, 5836. <https://doi.org/10.3390/app14135836>

Academic Editors: Reza Abedi and Stephanie TerMaath

Received: 5 June 2024

Revised: 25 June 2024

Accepted: 27 June 2024

Published: 3 July 2024



Copyright: © 2024 by the authors. Licensee MDPI, Basel, Switzerland. This article is an open access article distributed under the terms and conditions of the Creative Commons Attribution (CC BY) license (<https://creativecommons.org/licenses/by/4.0/>).

1. Introduction

The solid products generated by agriculture, and also those resulting from various industrial processes, are heterogeneous mixtures, i.e., mixtures of components with different characteristics or structures. To be marketed and subsequently used as raw materials in various processes, these products must undergo various operations, including mechanical separation [1–5].

The process of the mechanical separation of a heterogeneous mixture of solid particles can be carried out on surfaces provided with orifices, which, to make this process as efficient as possible, are subject to different types of movements, including the following [6–10]:

- Linear motion—with various types of mechanical devices, horizontal movement is imparted to a work surface to increase the efficiency of the sieving process and prevent smearing.
- Circular motion—this motion is generally found in vibrating screens with circular motion and is used for sorting particles into several fractions according to thickness or grain size or for sieving ground products with separation according to particle size.

- Elliptical movement—this is a combination of the two types of movement presented above, which is why its efficiency is much higher.
- Centrifugal motion—by imposing centrifugal motion on the mass of solid particles inside a perforated drum, the separation of a heterogeneous mixture into at least two fractions can be achieved.
- Gyroscopic motion—this requires highly efficient machines used in the long filtration processes of light particles, which use the gyroscopic motion generated by a series of vibrating motors.

The simplest and most commonly used method of driving a classic mechanical separator is the crank–rod or four-bar mechanism [11–14]. Depending on its position on the oscillating surface, and, more precisely, on the free end of the tie rod, different working conditions for this separator can be generated. This mechanism, with its four bars, is widely used because of its simplicity of construction, and according to the literature, it has been subjected to analyses using various methods [15–18].

The study of the influence of design parameters on mechanism kinematics is essential for several reasons. First, it allows engineers to better understand how different mechanisms work and how they can be improved to work more efficiently. Design parameters such as the size, shape, material, and position of the components of a mechanism can have significant impacts on how the functional parameters, such as the speed and acceleration of the mechanism, vary. For example, changing the dimensions of a mechanism element may improve or deteriorate its performance [19–21].

Second, understanding the influence of these parameters on mechanism kinematics can help design new mechanisms that are more efficient, durable, and reliable. This can lead to the development of new and better types of equipment that may be more attractive to users.

In general, a mechanism analysis is carried out using different methods, such as kinematic models [22–24], methods based on different calculation algorithms [25–27], mathematical synthesis [28], different mathematical models [29–31], etc. Depending on the reference system in which the study is to be carried out, an analysis can be carried out both planarly [32–36] and spatially [37–39].

Studies found in the specialized literature have also approached this field from the finite element point of view, and many simulations of the movements of different types of mechanisms have been identified [40–43].

Within the scientific literature, many comparative studies focused on several types of mechanisms, and the main purpose of these studies was to identify the movements they generated [44–48].

Also, according to the literature, many studies have determined the movement of the components of specific mechanisms using a very complex calculation that involves the analysis of each component of a mechanism [49–51].

This paper aimed to identify a six-bar mechanism that generated the same motion as a reference element, corresponding to a classical (four-bar) mechanism widely used in driving oscillating systems. This study started by identifying the trajectory of the free end of one component of the classical mechanism (i.e., the free end of the rocker arm). We kept only two reference elements of the classical mechanism (the crank and the tie rod/rocker arm) in addition to the other kinematic elements that were introduced into the mechanism, and these were arranged in such a way as to keep the same trajectory of the reference element (the final scheme of the mechanism used for the comparative analysis that was generated by the specialized program WATT [52]). The new mechanism obtained was theoretically analyzed in order to identify the movement of the components. At the end of this study, a comparative analysis of the operating characteristics between the classic mechanism (with four bars) and the new mechanism (with six bars) was carried out (i.e., the movement of the free end of the tie rod and its speed variation were analyzed comparatively). This study was also undertaken to identify the mathematical equations of motion of certain components of the six-bar mechanism. At the same time, because of

the existence of a small number of articles in the specialized literature (dealing with the analysis of this type of mechanism and the generalist mode of the equations obtained), we consider that this article represents an additional element in the enrichment of this theoretical and technical field.

2. Materials

As previously indicated, a variety of mechanical separators are utilized in order to perform size-based separation of a heterogeneous mixture of solid particles. The characteristics of the product undergoing the separation process (the size and shape of the particles in the mixtures, the density of the solid particles, the surface condition, etc.), as well as the type of surface used (a working surface made of different types of materials or made by different methods—by weaving or by stamping), are the factors that affect how the separation surface moves [11].

Oscillating screens (linear motion) are a common feature of various technological processes because of their numerous advantages. These include their simplicity of construction, relatively high feed rate, good displacement efficiency, and simple and low-cost operation and maintenance. For this reason, this article examines the movement of such a separator [53].

The initial stage of the investigation involved identifying the type of motion produced by the classical mechanism that drives an oscillating system. This mechanism is present in the majority of plane oscillating separators (Figure 1a) [53]. The conventional kinematic configuration of this type of mechanism is presented in Figure 1b, which features two rocker elements. Figure 1c illustrates the principle of the corresponding classical mechanism, which utilizes a single rocker element. This was created using Linkage software. The mechanism under investigation is composed of the following elements:

- Crank—represented as element AB, in both Figure 1b,c;
- Connecting rod—represented in Figure 1b as element BE and in Figure 1c as element BC;
- Tie rod—represented in Figure 1b as elements CD and GF, and in Figure 1c as element CD.

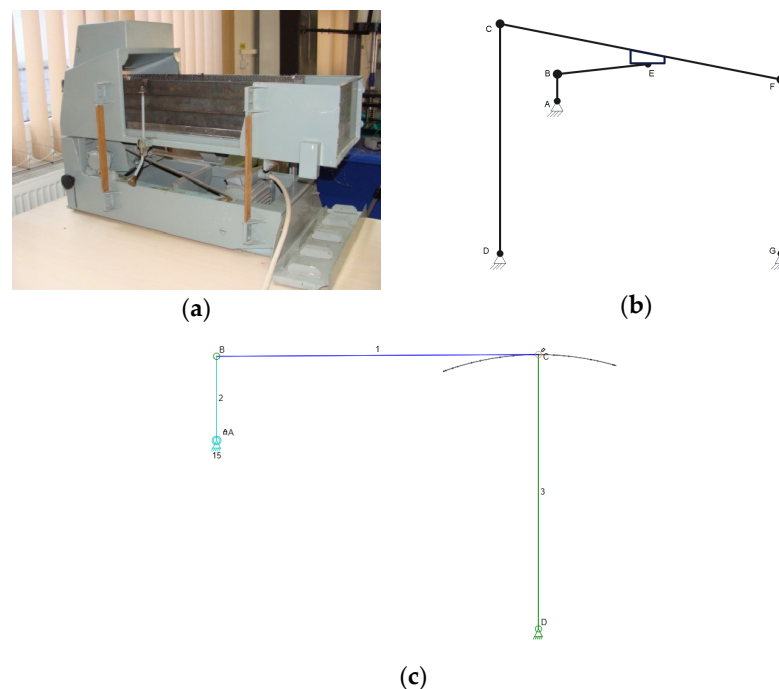


Figure 1. Four-bar mechanism: (a) the mechanical separator with oscillatory motion is designed for the separation of solid particles [53]; (b) a kinematic scheme for driving the oscillating surface; and (c) a schematic representation of the principle kinematic diagram of the corresponding four-bar mechanism: the letters A–G represent the couplings of the mechanisms; numbers 1–3 present the elements of the mechanism in Linkage software (they are presented above).

The study of the crank's action is uninteresting since it is a circular movement. Nevertheless, the movement of the rocker's arm is produced by this kinematic element through the connecting rod, and the trajectory it describes generates the movement that the oscillating surface performs. The geometrical analysis of this gearing has been discussed in various articles published in the scientific literature, including [53,54], which refer to it as the four-bar mechanism.

The trajectory of the tie rod, as illustrated in Figure 1 (which is shown in Figure 2), is the subject matter of our subsequent analysis. Based on this, we examined various systems that carry out the same action. The mechanism, illustrated in Figure 3 (the Stephenson mechanism with six bars), was selected from a total of 47 design options using the WATT software because of the resulting trajectory's high degree of similarity.

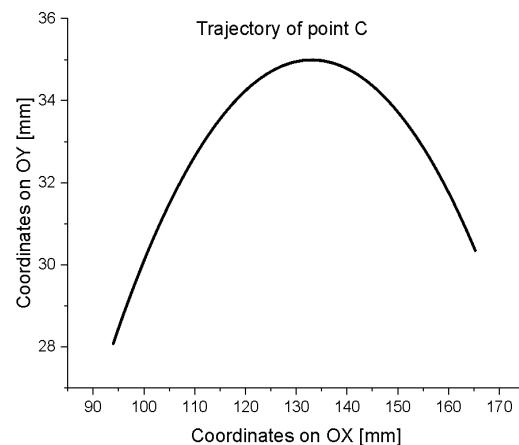


Figure 2. The trajectory that the free end of the tie rod describes.

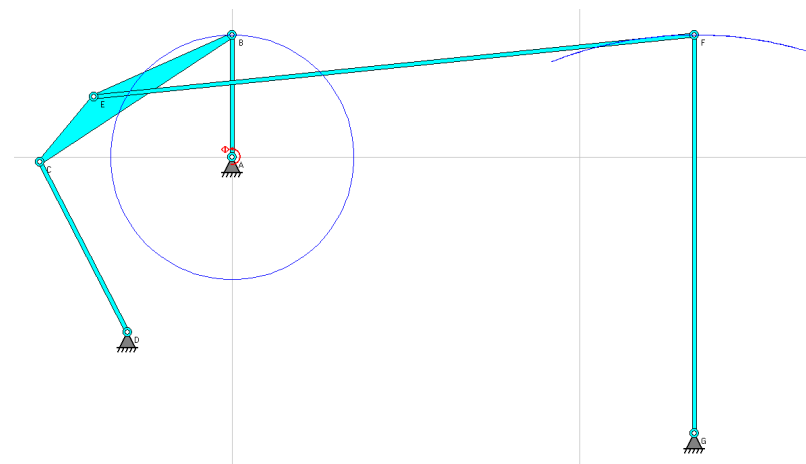


Figure 3. The mechanism under analysis (represented with the help of the Roberts program).

The mechanism chosen for study is a six-element mechanism (Figure 3), which comprises the following components:

- The AB element that cranks;
- The DC element, the left side rocker arm, represents a binary element;
- The CEB element, the connecting rod, represents a ternary element;
- The EF element that has the second connecting rod, which could materialize the movement trajectory of the oscillating screen;
- GF is the second rocker arm from the right side;
- The points A, . . . , G are located at the centers of the kinematic rotation couples.

3. Working Methodology

In order to analyze the movement of the components of the mechanism under investigation (the one shown in Figure 3), the following methodology was employed (Figure 4):

- First, the new mechanism's geometric coordinates for the couplings were determined (Figure 1);
- Several different programs were employed in order to facilitate a comparison of the outcomes of the checks carried out on the identified equations for many specified values. As previously noted, many software programs, each with a distinct function, were used:
- The shape of a new mechanism executing the movement under examination was determined using WATT v. 1.6.3. software (from Heron Technologies, Hoogeveen, The Netherlands) [55];
- The software Roberts v. 2.1.0 (from Heron Technologies, The Netherlands) was utilized to assess and visualize the motion produced by the mechanisms of this investigation, as well as to analyze and visualize the motion [56];
- The software called Linkage v. 3.11.3, created by David M. Rector, was utilized to confirm the accuracy of the motions generated by the mechanism [57];
- The mathematical computation of the relationships associated with the coordinates of the points under examination was carried out using the Mathcad v. 15 (PTC Mathcad) application [58];
- The graphical representations presented in this article were generated using OriginPro v. 9.6.5.169 (OriginLab Corporation, Northampton, MA, USA) [59].

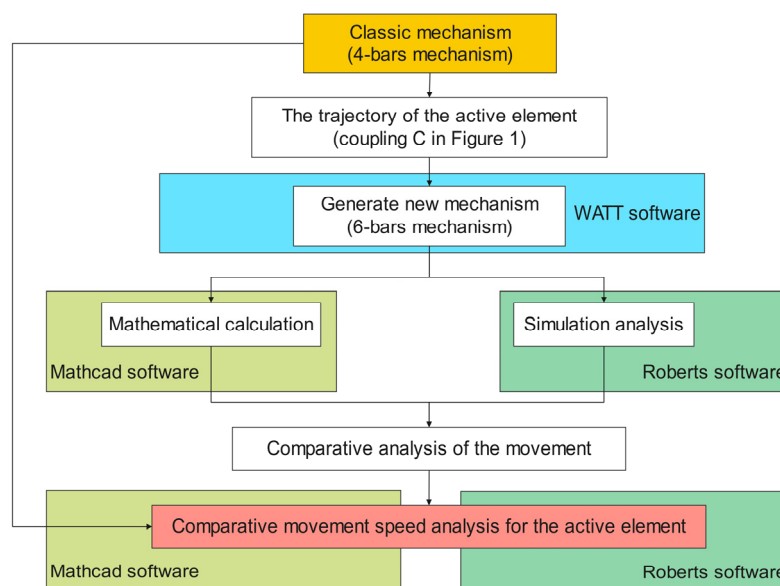


Figure 4. Methodology of the work.

4. Theoretical Considerations

The mechanism analyzed in this article is presented in Figure 5. It is a six-bar Stephenson mechanism.

As illustrated in Figure 5, the coordinates of coupling A (base A) are not provided, as this point was selected to be located at the origin of the coordinate system (i.e., at the center). Consequently, the coordinates of the other components of the mechanism were determined by taking this point into account.

In order to perform the requisite calculations, it was necessary to identify the following elements from a geometrical standpoint:

- The coordinates of fixed points were provided: D (x_0, y_0) and G (x_1, y_1);
- The dimensional values of the mechanism elements were as follows: AB— a ; BC— b ; CD— c ; BE— e ; CE— d ; EF— g ; FG— f ;

- The angle generated by the crank AB in relation to the horizontal (OX axis) was noted in the calculation with α ;
- The ECB ternary element was regarded as a rigid element.

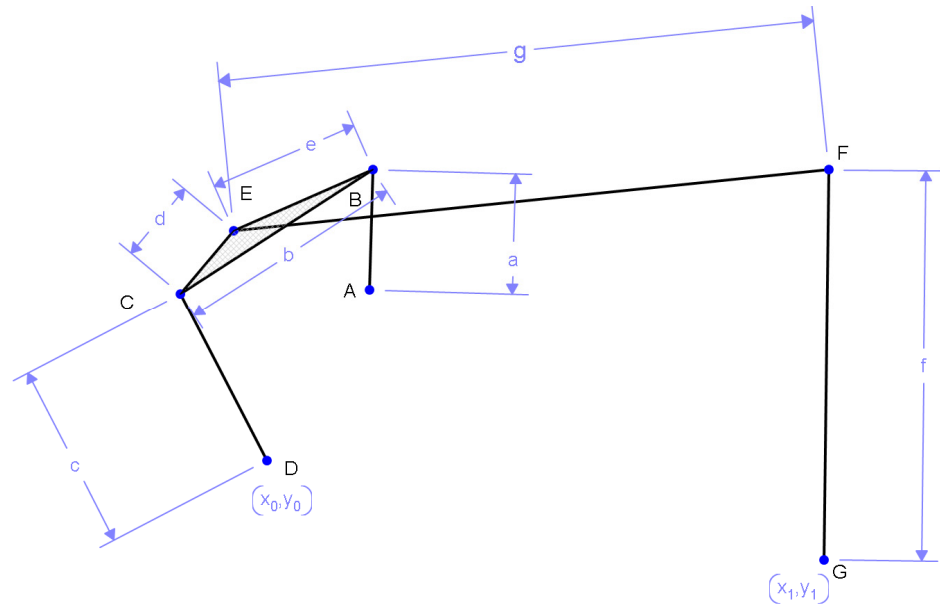


Figure 5. The components of the mechanism under study.

The geometrical analysis of the six-bar mechanism permitted the determination of the calculation relationships for the following kinematic torques: C, E, and F. The computational relationships of the kinematic torque coordinates, which were previously imposed, were obtained corresponding to the projection on the two axes OX and OY.

The results of the calculation relations, expressed in terms of the coordinates of the point in question, are displayed below:

- For coupling C (Equations (1) and (2)):

$$x_C = a \cdot \cos \alpha + \frac{(b^2 - c^2 + d_0^2) \cdot (x_0 - a \cdot \cos \alpha)}{2 \cdot d_0^2} - \frac{\sqrt{b+c+d_0} \cdot \sqrt{b+c-d_0} \cdot \sqrt{b-c+d_0} \cdot \sqrt{-b+c+d_0} \cdot (-y_0 + a \cdot \sin \alpha)}{2 \cdot d_0^2} \quad (1)$$

$$y_C = a \cdot \sin \alpha - \frac{\sqrt{b+c+d_0} \cdot \sqrt{b+c-d_0} \cdot \sqrt{b-c+d_0} \cdot \sqrt{-b+c+d_0} \cdot (-a \cdot \cos \alpha + x_0)}{2 \cdot d_0^2} + \frac{(b^2 - c^2 + d_0^2) \cdot (y_0 - a \cdot \sin \alpha)}{2 \cdot d_0^2} \quad (2)$$

- For coupling E (Equations (3) and (4)):

$$x_E = u_2 + \frac{(b^2 + d^2 - e^2) \cdot (-u_2 + a \cdot \cos \alpha)}{2 \cdot b^2} - \frac{\sqrt{b+d+e} \cdot \sqrt{b+d-e} \cdot \sqrt{b-d+e} \cdot \sqrt{-b+d+e} \cdot (v_2 - a \cdot \sin \alpha)}{2 \cdot b^2} \quad (3)$$

$$y_E = v_2 - \frac{\sqrt{b+d+e} \cdot \sqrt{b+d-e} \cdot \sqrt{b-d+e} \cdot \sqrt{-b+d+e} \cdot (a \cdot \cos \alpha - u_2)}{2 \cdot b^2} + \frac{(b^2 + d^2 - e^2) \cdot (-v_2 + a \cdot \sin \alpha)}{2 \cdot b^2} \quad (4)$$

- With regard to coupling F, the calculation equations are as follows (Equations (5) and (6)):

$$x_F = u_3 + \frac{(-f^2 + g^2 + d_5^2) \cdot (x_1 - u_3)}{2 \cdot d_5^2} + \frac{\sqrt{f+g+d_5} \cdot \sqrt{f+g-d_5} \cdot \sqrt{f-g+d_5} \cdot \sqrt{-f+g+d_5} \cdot (-y_1 + v_3)}{2 \cdot d_5^2} \quad (5)$$

$$y_F = v_3 + \frac{\sqrt{f+g+d_5} \cdot \sqrt{f+g-d_5} \cdot \sqrt{f-g+d_5} \cdot \sqrt{-f+g+d_5} \cdot (x_1 - u_3)}{2 \cdot d_5^2} + \frac{(-f^2 + g^2 + d_5^2) \cdot (y_1 - v_3)}{2 \cdot d_5^2} \tag{6}$$

Because of the considerable sizes of the equations obtained (for the determination of the coordinates of the three analyzed couples), a series of sub-annotations were made (Equations (7)–(15)) as follows:

$$d_o = \sqrt{(-x_o + a \cdot \cos \alpha)^2 + (-y_o + a \cdot \sin \alpha)^2} \tag{7}$$

$$d_2 = \sqrt{b+c+d_o} \cdot \sqrt{b+c-d_o} \cdot \sqrt{b-c+d_o} \cdot \sqrt{-b+c+d_o} \tag{8}$$

$$u_2 = a \cdot \cos \alpha + \frac{(b^2 - c^2 + d_o^2) \cdot (-a \cdot \cos \alpha + x_o)}{2 \cdot d_o^2} - \frac{d_2 \cdot (-y_o + a \cdot \sin \alpha)}{2 \cdot d_o^2} \tag{9}$$

$$v_2 = a \cdot \sin \alpha - \frac{d_2 \cdot (x_o - a \cdot \cos \alpha)}{2 \cdot d_o^2} + \frac{(b^2 - c^2 + d_o^2) \cdot (-a \cdot \sin \alpha + y_o)}{2 \cdot d_o^2} \tag{10}$$

$$d_4 = \sqrt{b+d+e} \cdot \sqrt{b+d-e} \cdot \sqrt{b-d+e} \cdot \sqrt{-b+d+e} \tag{11}$$

$$u_3 = u_2 + \frac{(b^2 + d^2 - e^2) \cdot (a \cdot \cos \alpha - u_2)}{2 \cdot b^2} - \frac{d_4 \cdot (v_2 - a \cdot \sin \alpha)}{2 \cdot b^2} \tag{12}$$

$$v_3 = v_2 + \frac{d_4 \cdot (-u_2 + a \cdot \cos \alpha)}{2 \cdot b^2} + \frac{(b^2 + d^2 - e^2) \cdot (a \cdot \sin \alpha - v_2)}{2 \cdot b^2} \tag{13}$$

$$d_5 = \sqrt{(-x_1 + u_3)^2 + (-y_1 + v_3)^2} \tag{14}$$

$$d_6 = \sqrt{f+g+d_5} \cdot \sqrt{f+g-d_5} \cdot \sqrt{f-g+d_5} \cdot \sqrt{-f+g+d_5} \tag{15}$$

The final forms of the equations describing the motion of the torques were calculated by replacing the terms contained in Equations (7)–(15) into Equations (1)–(6) and carrying out the corresponding solving and reduction of the terms, from a mathematical perspective as follows:

- For coupling C (Equations (16) and (17)):

$$x_C = a \cdot \cos \alpha + \frac{(b^2 - c^2 + d_o^2) \cdot (x_o - a \cdot \cos \alpha)}{2 \cdot d_o^2} - \frac{d_2 \cdot (-y_o + a \cdot \sin \alpha)}{2 \cdot d_o^2} \tag{16}$$

$$y_C = a \cdot \sin \alpha - \frac{d_2 \cdot (-a \cdot \cos \alpha + x_o)}{2 \cdot d_o^2} + \frac{(b^2 - c^2 + d_o^2) \cdot (y_o - a \cdot \sin \alpha)}{2 \cdot d_o^2} \tag{17}$$

- For coupling E (Equations (18) and (19)):

$$x_E = u_2 + \frac{(b^2 + d^2 - e^2) \cdot (-u_2 + a \cdot \cos \alpha)}{2 \cdot b^2} - \frac{d_4 \cdot (v_2 - a \cdot \sin \alpha)}{2 \cdot b^2} \tag{18}$$

$$y_E = v_2 - \frac{d_4 \cdot (a \cdot \cos \alpha - u_2)}{2 \cdot b^2} + \frac{(b^2 + d^2 - e^2) \cdot (-v_2 + a \cdot \sin \alpha)}{2 \cdot b^2} \tag{19}$$

- For coupling F (Equations (20) and (21)):

$$x_F = u_3 + \frac{(-f^2 + g^2 + d_5^2) \cdot (x_1 - u_3)}{2 \cdot d_5^2} + \frac{d_6 \cdot (-y_1 + v_3)}{2 \cdot d_5^2} \tag{20}$$

$$y_F = v_3 + \frac{d_6 \cdot (x_1 - u_3)}{2 \cdot d_5^2} + \frac{(-f^2 + g^2 + d_5^2) \cdot (y_1 - v_3)}{2 \cdot d_5^2} \tag{21}$$

5. Results

In order to perform the analytical validation of the obtained equations (Equations (16)–(21)), the following set of component values was utilized. It should be noted that whilst some of these components are shared by the two mechanisms discussed in this article, they do not match the constructive elements found in real equipment. Furthermore, the values were only utilized to confirm the precision of the mathematical relationships.

- In the case of both mechanisms, the coordinates of point A are (0,0);
- The dimensional value of the crank, i.e., the AB element, is 35 mm (for both the four-bar and six-bar mechanisms);
- The coordinates of the point corresponding to the tie rod bearing, which in Figure 1 is denoted by D and in Figures 3 and 5 by G, are (133, -79);
- The size of the tie rod for both mechanisms is 114 mm (element FG in Figures 3 and 5 or element DC in Figure 1);
- The dimensional value used for the connecting rod corresponding to Figure 1, i.e., the value of the CB element, is 133 mm. In contrast, the value corresponding to the same component but in Figure 3 is 174 mm;
- Figure 5 shows the distinctive components of the six-bar mechanism:
- The following dimensional values define the ternary element BCE: element BC = 67 mm; element CE = 24 mm; and element EB = 44 mm;
- The binary element CD has a value of 55 mm.

The use of the Mathcad 15 program, a valuable tool for engineers engaged in the analysis of mechanisms, enabled us to perform mathematical calculations corresponding to the equations obtained (i.e., Equations (16)–(21)) from a mathematical standpoint. The use of the Mathcad 15 program can facilitate the simplification and improvement of the kinematic analysis process.

The trajectories, corresponding to torques C and E, are presented in Figure 6a,b. These values were calculated by substituting the previously mentioned terms in the calculation Equations (16)–(19).

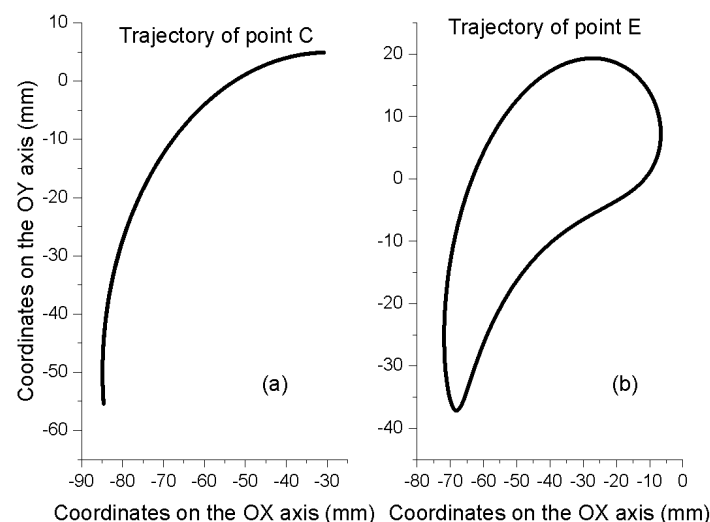


Figure 6. (a) The trajectory that coupling C describes. (b) The trajectory that coupling F describes.

A comparison of the two trajectories reveals the following:

- The trajectory of coupling C is represented by a circular arc, which is a consequence of the fact that one of the ends of the binary element DC is a fixed element (i.e., coupling D);
- The trajectory of coupling E is a complex trajectory, which is a consequence of the fact that the ternary element BCE is connected at the ends (i.e., in couplings C and B) to

the binary elements CD and AB, which have a fixed end, and to the binary element EF which is mobile.

With regard to the trajectory corresponding to point F (as illustrated in Figure 5) the results obtained were subjected to analysis by comparing the values obtained using two distinct software programs including the following:

1. Mathcad [58]—in this program, the trajectory of point F was calculated using mathematical methods;
2. Roberts [56]—this software is designed for the simulation of the movement of the mechanism with six bars, which allows for the determination of the trajectory of point F.

Figure 7 displays a comparison of the trajectories, represented by point F, that were produced by the two work programs utilized.

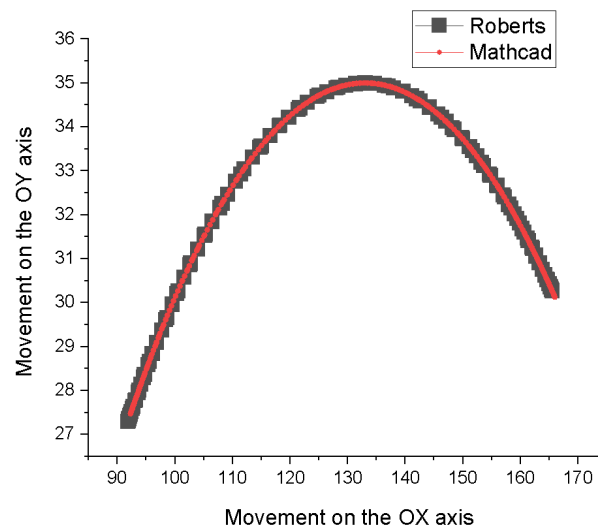


Figure 7. A comparative analysis of the trajectory of point F.

The graphical representation analysis, see Figure 7, indicates that the results obtained mathematically are comparable to those obtained using the Roberts simulation program. However, a minor discrepancy is observed on the left side of the trajectory, with a difference of 0.45 mm on the OX axis and 0.17 mm on the OY axis.

Furthermore, the displacement speed of point F can be calculated using the same programs. This comparative variation is illustrated in Figure 8.

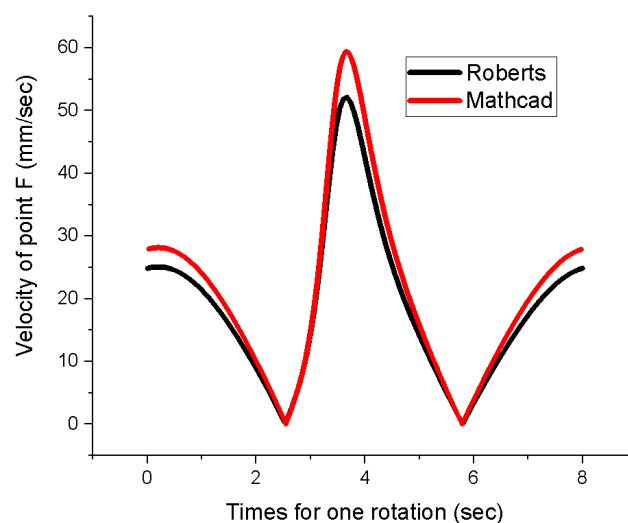


Figure 8. The variation in the speed of point F's movement.

The difference between the two sets of values, which describe the linear velocity variation corresponding to point F, is illustrated in Figure 9. The values obtained from the Roberts simulation software and those derived from the mathematical computation (using Mathcad 15 [58]) were subtracted to create this graphical representation. This suggests there is a maximum difference of 2 mm/s between the two sets of values.

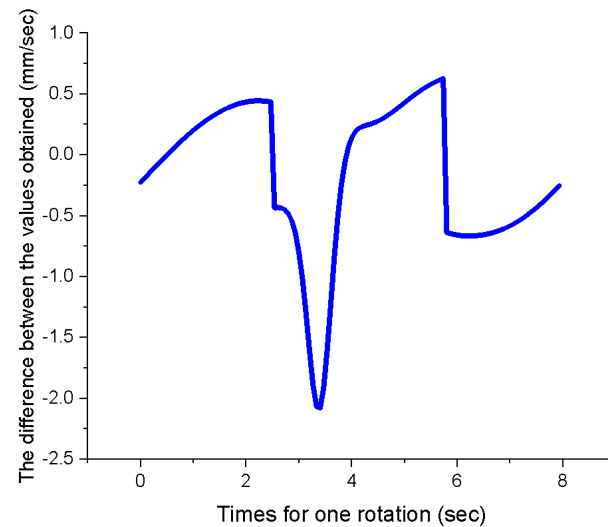


Figure 9. The difference between the two methods for determining the velocity of the movement of point F.

The principal objective of this study is to identify a mechanism that generates the same motion as that produced by a classical mechanism, which will then be employed in the drive of an oscillating separator used for the mechanical separation process. The following analysis therefore concerns the movement executed by the literal end of the tie rod (the FG element in Figure 5) generated by the mechanism under analysis (six-bar mechanism) and by the classical mechanism (the DC element in Figure 1) found in the various types of mechanical separators operating oscillating screens (four-bar mechanism). For this reason, Figure 10 compares the trajectory produced by the six-bar mechanism (for which the values obtained using the mathematical calculation and the results obtained with the Mathcad program were used [58]) with the trajectory described by the four-bar mechanism obtained using a torque study in the Roberts simulation program (the simulation took into account the constructive characteristics presented at the beginning of this section).

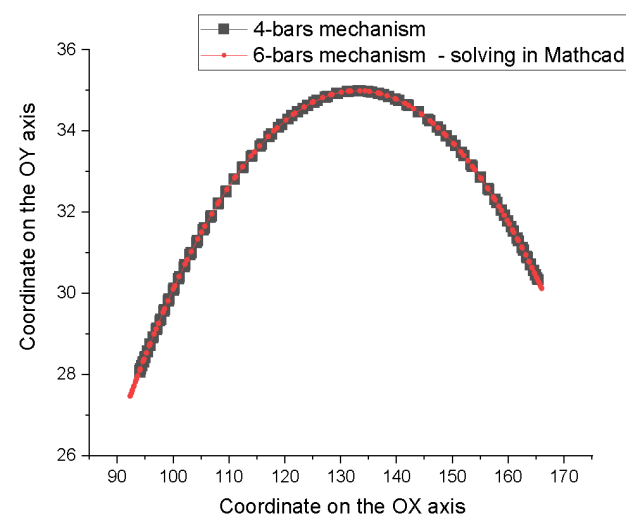


Figure 10. A comparison of the trajectories of the tie rod's free end for the two mechanisms under study.

As illustrated in Figure 7, there is a distinction between the two trajectories in this specific case. This discrepancy can only be discerned between the two endpoints of the trajectory as follows:

- It can be observed that the difference between the endpoints of the trajectory on the right-hand side is 0.35 mm for the OX axis and 0.18 mm for the OY axis;
- For the left side of the trajectories, the difference between the two ends is 1.317 mm for the OX axis and 1.493 mm for the OY axis.

The trajectory generated by the movement of the free end of the tie rod, for the mechanism with six bars, was found to be 5 mm greater than that of the mechanism with four bars. It is important to note that the movement of the free end of the tie rod, for the four-bar mechanism, was identified using the Roberts program.

A graphical comparison of the velocities obtained for the two oscillatory motion-generating systems under examination is presented in Figure 11. The data presented in Figure 10 were obtained using the programs shown above, namely, Mathcad [58] and Roberts [56]. The representation was performed in accordance with the mechanism representation mode (Figures 1 and 3). The value 0 in the graphical representation is indicative of the starting position of the mechanism analysis, namely, the crank handle. The result of the change can be observed by analyzing the representation of the change in the speed of the movement of the tie rod's free end as follows:

- In the range of 270° to 90° (upper dial) (analysis performed in a counterclockwise direction), the two defining elements, namely, the linear velocity variation and the angular value corresponding to this velocity, are found to be close for the two mechanisms under comparison. The difference between the maximum values is 2.39 mm/s with an angular offset of 12° ;
- For the same direction of movement, but for the lower dial, i.e., that corresponding to the range of 90 – 270° , the variation curves of the speed of movement of the free end of the tie rod differ for the two mechanisms analyzed. The maximum speed obtained for the four-bar mechanism is 31.69 mm/s, while the six-bar mechanism is 20.48 mm/s higher. Furthermore, the angular difference between the maximum speed values is 48 degrees. The maximum speed value of the six-bar mechanism is observed within the 90 – 180° quadrant, while the maximum speed value of the four-bar mechanism is observed within the 180 – 270° quadrant. This element is of great importance for the drive mode of the oscillating site, as it is characterized by the pulling action of the entire assembly by the crank in the 90 – 180° dial and by the crank pushing the entire mechanical assembly in the 180 – 270° dial.

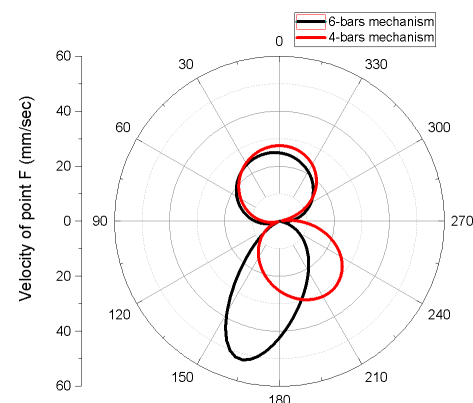


Figure 11. Variation in the linear speed of the free end of the tie rod.

This discrepancy in values is attributable to the drive system of the F element, specifically, the constructive dimension represented by the “crank-rod” mechanism and the speed of movement of the free end of the tie rod as follows:

- The classical mechanism (with four bars) is characterized by the size of the elements AB and BC (Figure 1);
- The six-bar mechanism under analysis is characterized by the entire structure formed by the following elements: binary—AB; ternary—BCE; binary CD; and binary EF (Figure 3);
- When analyzing the two drive systems, it is clear that the drive components in Figures 1 and 3 have different constructional characteristics, and when examining the final torque, the following is evident:
- The distance between couplings A and B for the four-bar mechanism is constant and it is equal to 35 mm;
- The distance between couplings A and E, for the six-bar mechanism, is variable and can be determined using Equation (22).

$$l_{AE} = \sqrt{\left(u_2 + \frac{(b^2+d^2-e^2) \cdot (-u_2+a \cdot \cos\alpha)}{2 \cdot b^2} - \frac{d_4 \cdot (v_2-a \cdot \sin\alpha)}{2 \cdot b^2}\right)^2 + \left(v_2 - \frac{d_4 \cdot (-u_2+a \cdot \cos\alpha)}{2 \cdot b^2} + \frac{(b^2+d^2-e^2) \cdot (-v_2+a \cdot \sin\alpha)}{2 \cdot b^2}\right)^2} \quad (22)$$

Since point A was assumed to be at the origin of the coordinate system (i.e., has coordinates (0,0)), by using Equations (18) and (19), we obtain Equation (23):

$$l_{AE} = \sqrt{(x_E)^2 + (y_E)^2} \quad (23)$$

The graph in Figure 12 shows the variation in the distance between couplings A and E, which, as can be seen from the representation, can have a minimum value of 9.38 mm and a maximum value of 79.39 mm.

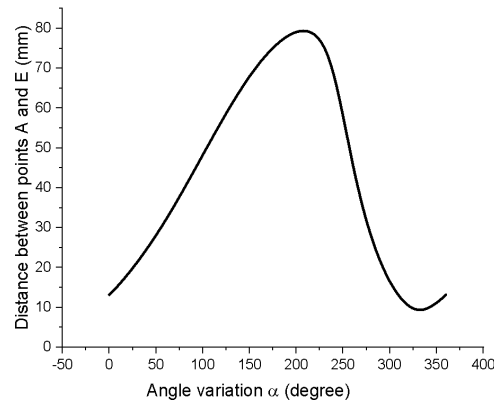


Figure 12. Variations in the distance between couplings A and E.

6. Conclusions

The use of agro-industrial raw materials to obtain a series of products requires prior mechanical pre-processing with the required mechanical characteristics. For this purpose, several tools have been developed to clean, sort, and categorize agro-industrial products. Mechanical separators with perforated working surfaces are the most frequently utilized equipment of this type. They can perform a series of simple or complex movements that increase the process's efficiency.

The motions of the separating surfaces are generated by many mechanisms. These have been studied in the literature in a variety of ways.

The most widely used mechanism, in this field and beyond is the four-bar mechanism. For this reason, we attempted to find a different and more complex mechanism that produces the same movement in the present paper.

After analysis using WATT, a program for generating different types of mechanisms, it was decided to use a six-bar mechanism (Figure 3).

As a result of the analysis, from a geometrical point of view, it was possible to determine the calculation equations corresponding to the kinematic torques C, E, and F (Equations (16)–(21)). For these elements, using the equations identified, it was possible to draw the curves they generate, obtaining (Figure 6) simple curves (circular arc for torques C and F) and complex curves (for torque E).

In an effort to confirm the precision of the results, from a mathematical point of view, a parallel study was conducted using Roberts software to simulate the movement of the mechanism. The investigation revealed that there are no significant differences between the mathematical calculations performed and the simulation of the movement of the six-bar mechanism (Figure 7).

In addition, using comparative analysis, the two mechanisms studied were analyzed in terms of the distance traveled by the reference element (the free end of the connecting rod), and the following conclusions were drawn:

- For the classical mechanism (the one with four bars) the trajectory generated by the Roberts simulation program was chosen;
- For the six-bar mechanism, the trajectory resulting from the mathematical calculation was chosen;
- The difference between the two trajectories generated by the two mechanisms is 5 mm.

This theoretical study also involved an analysis of the variation in the speed of the kinematic element for the two different types of mechanisms (Figures 8 and 9). This analysis revealed a significant differentiation in the velocity in the lower part of the dial representing the variation in this parameter (Figure 10), which is reflected in the position where this parameter has its maximum value as well as in the difference in its maximum value.

The mechanism generated by the WATT program (the six-bar mechanism) generates a high value of the kinematic element velocity F (Figure 10) (the one to which the oscillating sieve is attached), which imposes an increased velocity on the sieving surface, i.e., in the mass of solid particles. This provides information on the effect of the kinematic element velocity value on the mechanical separation process. From a theoretical point of view, it follows that for the same mass on solid particles located on the separation surface, their velocity in the case of the six-bar mechanism is higher than in the case of the classical mechanism. This does not mean that the mechanism is better or worse than the classical mechanism currently in use. Several practical studies need to be carried out to establish this.

This work differs from those in the literature in that it provides mathematical equations for the motion generated by kinematic couplings. These equations were obtained taking into account all dimensional components of the mechanism and presented as a whole and were not made for structural groups of components of the mechanism. The main relations obtained (Equations (16)–(21)) are intended to help us in the design and realization of a much simpler mechanism—with six bars—by using a single calculation relation specific to a certain coordinate compared with the literature where step-by-step analysis of the mechanism is applied, generating many calculation relations [60–63].

This article did not study the impact that the speed of the driving element (of the crank handle) in the real case (where the speed of this element can be over 150 rpm) has on the wear of the components of the complex mechanism.

This study will be continued with the aim of identifying (also from a theoretical point of view) other types of mechanisms that can be used for the same purpose of generating oscillatory motion for mechanical separators found in different process industries. We will also examine the impact of the design elements on the way the motion of the components under study is achieved.

Author Contributions: Conceptualization, E.M. and L.B.; methodology, E.M.; software, E.M.; validation, M.J., G.P. and N.S.; formal analysis, M.P.-L.; data curation, E.M.; writing—original draft preparation, E.M. and M.P.-L.; writing—review and editing, D.C.; visualization, M.J. and G.P.; supervision, M.J. and N.S. All authors have read and agreed to the published version of the manuscript.

Funding: This research received no external funding.

Institutional Review Board Statement: Not applicable.

Informed Consent Statement: Not applicable.

Data Availability Statement: The raw data supporting the conclusions of this article will be made available by the corresponding author on request.

Conflicts of Interest: The authors declare no conflicts of interest.

References

1. Alessi, A.; Lopes, A.D.P.; Müller, W.; Gerke, F.; Robra, S.; Bockreis, A. Mechanical separation of impurities in biowaste: Comparison of four different pretreatment systems. *Waste Manag.* **2020**, *106*, 12–20. [[CrossRef](#)] [[PubMed](#)]
2. Lyons, G.A.; Cathcart, A.; Frost, J.P.; Wills, M.; Johnston, C.; Ramsey, R.; Smyth, B. Review of two mechanical separation technologies for the sustainable management of agricultural phosphorus in nutrient-vulnerable zones. *Agronomy* **2021**, *11*, 836. [[CrossRef](#)]
3. Mosnegutu, E.; Chitimus, A.D.; Barsan, N.; Rusu, D.; Vulpe, M.; Nedeff, V.; Jasinski, M. Studies and researches regarding the influence of the size of solid particles forming a heterogenous mix on the aerodynamic separation process. In Proceedings of the 7th International Conference on Energy Efficiency and Agricultural Engineering (Ee&Ae), Ruse, Bulgaria, 11–13 June 2020.
4. Müssig, J.; Enke, S.; Gusovius, H.; Lühr, C.; Uhrlaub, B.; Dammer, L.; Carus, M. Mechanical separation of kenaf for composite applications—Evaluation of the total fibre line concept for field retted kenaf. *Ind. Crops Prod.* **2024**, *208*, 117870. [[CrossRef](#)]
5. Saravacos, G.; Kostaropoulos, A.E. Mechanical separation equipment. In *Handbook of Food Processing Equipment*; Springer: Cham, Switzerland, 2016; pp. 233–292. [[CrossRef](#)]
6. Chaugule, V.; Narayanaswamy, R.; Lucey, A.D.; Narayanan, V.; Jewkes, J. Particle image velocimetry and infrared thermography of turbulent jet impingement on an oscillating surface. *Exp. Therm. Fluid Sci.* **2018**, *98*, 576–593. [[CrossRef](#)]
7. Mosnegutu, E.F.; Nedeff, V.; Barsan, N.; Sandu, I.; Panainte-Lehadus, M.; Chitimus, D.; Sandu, I.G.; Bontas, O.; Rusu, D.I.; Topan, G. Application in process industry of the solid particles displacement on a flat oscillating surface. *Rev. De Chim.* **2020**, *71*, 42–50. [[CrossRef](#)]
8. Krishna, J. Gyro Screen—Screening and Separating Equipment. Available online: <https://www.jkmagnetic.com/gyro-screening-and-separating-equipment/> (accessed on 30 May 2024).
9. Chen, Z.; Tong, X.; Li, Z. Numerical Investigation on the sieving performance of elliptical vibrating screen. *Processes* **2020**, *8*, 1151. [[CrossRef](#)]
10. Dreyer, C.B.; Walton, O.; Riedel, E.P. Centrifugal sieve for size-segregation and beneficiation of regolith. *Earth Space* **2012**, *2012*, 31–35. [[CrossRef](#)]
11. Bontas, O.; Nedeff, V.; Mosnegutu, E.F.; Panainte, M.; Irimia, O.T. Behaviour of solid particles on a flat oscillating surface. *Environ. Eng. Manag. J.* **2013**, *12*, 17–22. [[CrossRef](#)]
12. Ahmedalbashir, M.; Romdhane, L.; Lee, J. Dynamics of a four-bar mechanism with clearance and springs—Modeling and experimental analysis. *J. Mech. Sci. Technol.* **2017**, *31*, 1023–1033. [[CrossRef](#)]
13. Akhadkar, C.A.; Deoghare, A.B.; Vaidya, A.M. Simulation and experimental response of four-bar mechanism with tolerance stack. *J. Mech. Eng. Sci.* **2019**, *13*, 4512–4535. [[CrossRef](#)]
14. De Jong, J.J.; Aarts, R.G.K.M. Static balance of a flexure-based four-bar mechanism: Less torque with more preload. *Adv. Serv. Ind. Robot.* **2022**, *120*, 306–313. [[CrossRef](#)]
15. Jaiswal, A.; Jawale, H.P. Synthesis and optimization of four bar mechanism with six design parameters. *Adv. Mech. Des. Mater. Manuf.* **2018**, *1943*, 020014. [[CrossRef](#)]
16. Kanna, G.R.; Ashik, M. Design and development of a rope climbing robot using four bar mechanism with wireless control using TX2/RX2 RF module. In Proceedings of the 2015 IEEE International Conference on Signal Processing, Informatics, Communication and Energy Systems (Spices), Kozhikode, India, 19–21 February 2015.
17. Peón-Escalante, R.; Flota-Bañuelos, M.; Quintal-Palomo, R.; Ricalde, L.J.; Peñuñuri, F.; Jiménez, B.C.; Viñas, J.A. Neural network based control of four-bar mechanism with variable input velocity. *Mathematics* **2023**, *11*, 2148. [[CrossRef](#)]
18. Rodríguez-Molina, A.; Villarreal-Cervantes, M.G.; Aldape-Pérez, M. A Dynamic optimization approach to adaptive control for the four-bar linkage mechanism. *Adv. Intell. Syst.* **2019**, *869*, 892–906. [[CrossRef](#)]
19. Moşnegutu, E.; Nedeff, V.; Birsan, N.; Chitimus, A.-D.; Rusu, D. Influence of screening block supporting way on the behaviour of a solid particle on an oscillating surface. *J. Eng. Stud. Res.* **2016**, *21*, 51–58. [[CrossRef](#)]
20. Iqbal, A.; Veer, S.; Gu, Y. Analytical solution to a time-varying LIP model for quadrupedal walking on a vertically oscillating surface. *Mechatronics* **2023**, *96*, 103073. [[CrossRef](#)]
21. Mosnegutu, E.; Nedeff, V.; Bontas, O.; Barsan, N.; Chitimus, D.; Rusu, D. Determination of kinematic indices corresponding to a solid particle on a flat oscillating surface. *IOP Conf. Ser. Mater. Sci. Eng.* **2016**, *147*, 012151. [[CrossRef](#)]
22. Escobar, L.; Bolanos, E.; Bravo, X.; Comina, M.; Hidalgo, J.L.; Ibarra, A. Kinematic resolution of delta robot using four bar mechanism theory. In Proceedings of the 2017 IEEE International Conference on Mechatronics and Automation (ICMA), Takamatsu, Japan, 6–9 August 2017; pp. 881–887.

23. Sabzali, H.; Koochakzadeh, E.; Moradi, A.; Akbarzadeh, A. Kinematics and dynamics optimization of a novel non-circular gear-attached four-bar mechanism for knee exoskeleton robot. In Proceedings of the 2022 10th Rsi International Conference on Robotics and Mechatronics (ICROM), Tehran, Iran, 15–18 November 2022; pp. 190–195. [\[CrossRef\]](#)
24. El-Shakery, S.; Ramadan, R.; Khader, K. Analytical and graphical optimal synthesis of crank-rocker four bar mechanisms for achieving targeted transmission angle deviations. *Jordan J. Mech. Ind. Eng.* **2020**, *14*, 303–313.
25. Boskovic, M.; Bulatovic, R.R.; Salinic, S.; Miodragovic, G.R.; Bogdanovic, G.M. Optimization of dynamic quantities of a four-bar mechanism using the Hybrid Cuckoo Search and Firefly Algorithm (H-CS-FA). *Arch. Appl. Mech.* **2018**, *88*, 2317–2338. [\[CrossRef\]](#)
26. Flores-Pulido, L.; Portilla-Flores, E.A.; Santiago-Valentin, E.; Vega-Alvarado, E.; Yanez, M.B.C.; Nino-Suarez, P.A. A comparative study of improved harmony search algorithm in four bar mechanisms. *IEEE Access* **2020**, *8*, 148757–148778. [\[CrossRef\]](#)
27. Qaiyum, A.; Mohammad, A. A novel approach for optimal synthesis of path generator four-bar planar mechanism using improved harmony search algorithm. *Aust. J. Mech. Eng.* **2024**, *22*, 95–108. [\[CrossRef\]](#)
28. Wang, B.; Du, X.C.; Ding, J.Z.; Dong, Y.; Wang, C.J.; Liu, X.A. The synthesis of planar four-bar linkage for mixed motion and function generation. *Sensors* **2021**, *21*, 3504. [\[CrossRef\]](#) [\[PubMed\]](#)
29. Bandopadhyaya, D.; Njuguna, J. Modelling and analysis of an ionic polymer-metal composite (IPMC)-rocker-based four-bar for variable path generation using the Euler-Bernoulli approach. *Proc. Inst. Mech. Eng. Part C J. Mech. Eng. Sci.* **2009**, *223*, 2405–2411. [\[CrossRef\]](#)
30. Cakar, O.; Tanyildizi, A.K. Application of moving sliding mode control for a DC motor driven four-bar mechanism. *Adv. Mech. Eng.* **2018**, *10*, 1687814018762184. [\[CrossRef\]](#)
31. Ge, Q.J.; Purwar, A.; Zhao, P.; Deshpande, S. A Task-driven approach to unified synthesis of planar four-bar linkages using algebraic fitting of a pencil of G-manifolds. *J. Comput. Inf. Sci. Eng.* **2017**, *17*, 031011. [\[CrossRef\]](#)
32. Arman, R.; Mahyuddin, A.I.; Marthiana, W.; Satria, I. Experimental investigation of vibration response of a flexible coupler in a four bar mechanism due to varying crank length and crank speed. In Proceedings of the 4th Engineering Science and Technology International Conference (Estic 2018), Padang, Indonesia, 28–29 August 2018; Volume 248, p. 01008. [\[CrossRef\]](#)
33. Diab, N. A new graphical technique for acceleration analysis of four bar mechanisms using the instantaneous center of zero acceleration. *SN Appl. Sci.* **2021**, *3*, 327. [\[CrossRef\]](#)
34. Kadak, T.; Kiper, G. Function generation with planar four-bar mechanisms as a mixed problem of correlation of crank angles and dead center design. *Sādhanā* **2024**, *49*, 143. [\[CrossRef\]](#)
35. Meijaard, J.P.; van der Wijk, V. Principal vectors and equivalent mass descriptions for the equations of motion of planar four-bar mechanisms. *Multibody Syst. Dyn.* **2020**, *48*, 259–282. [\[CrossRef\]](#)
36. Zhang, L.; Hu, K.W.; Tu, C.Y. Design methods of planar six-bar mechanism in servo applications. *J. Chin. Inst. Eng.* **2022**, *45*, 569–578. [\[CrossRef\]](#)
37. Bustamante, M.; Vega-Centeno, R.; Sánchez, M.; Mio, R. A parametric 3D-printed body-powered hand prosthesis based on the four-bar linkage mechanism. In Proceedings of the 2018 IEEE 18th International Conference on Bioinformatics and Bioengineering (BIBE), Taichung, Taiwan, 29–31 October 2018; pp. 79–85. [\[CrossRef\]](#)
38. Guo, X.N.; Chu, J.K. The rotatability of Stephenson ii six-bar mechanisms. In Proceedings of the 32nd Annual Mechanisms and Robotics Conference, Brooklyn, NY, USA, 3–6 August 2008; pp. 591–595. [\[CrossRef\]](#)
39. Liu, Y.; Yang, S. Kinematic solution of spherical Stephenson-III six-bar mechanism. *Chin. J. Mech. Eng.* **2013**, *26*, 851–860. [\[CrossRef\]](#)
40. Attia, E.M.; Abd El-Naem, M.A.; El-Gamal, H.A.; Awad, T.H.; Mohamed, K.T. Simulation of the motion of a four bar prosthetic knee mechanism fitted with a magneto-rheological damper. *J. Vibroeng.* **2016**, *18*, 4051–4068. [\[CrossRef\]](#)
41. Mo, X.J.; Ge, W.J.; Wang, S.C.; Zhao, D.L. Mechanical design and dynamics simulation of locust-inspired straight line four-bar jumping mechanism. *Lect. Notes Electr. Eng.* **2017**, *408*, 429–442. [\[CrossRef\]](#)
42. Sharifgalieva, I. The Design and Simulation of Mechanisms. Master's Thesis, Arcada University of Applied Sciences, Helsinki, Finland, 2018; pp. 1–61.
43. Zhang, K.; Yang, M.W.; Zhang, Y.M.; Huang, Q.J. Error feedback method (EFM) based dimension synthesis optimisation for four-bar linkage mechanism. *Appl. Soft Comput.* **2023**, *144*, 110424. [\[CrossRef\]](#)
44. Soh, G.S.; Ying, F.; McCarthy, J.M. Dimensional synthesis of planar six-bar linkages by mechanically constrain a prr serial chain. In Proceedings of the ASME 2012 International Design Engineering Technical Conferences & Computers and Information in Engineering Conference IDETC/CIE 2012, Chicago, IL, USA, 12–15 August 2012; pp. 1–7.
45. Chung, W.-Y. Double configurations of five-link Assur kinematic chain and stationary configurations of Stephenson six-bar. *Mech. Mach. Theory* **2007**, *42*, 1653–1662. [\[CrossRef\]](#)
46. Hu, J.; Sun, Y.; Cheng, Y. High mechanical advantage design of six-bar Stephenson mechanism for servo mechanical presses. *Adv. Mech. Eng.* **2016**, *8*, 1687814016656108. [\[CrossRef\]](#)
47. Lanese, N.A.; Myszka, D.H.; Bazler, A.L.; Murray, A.P. Six-bar linkage models of a recumbent tricycle mechanism to increase power throughput in FES cycling. *Robotics* **2022**, *11*, 26. [\[CrossRef\]](#)
48. Pieber, M.; Gerstmayr, J. Six-bar linkages with compliant mechanisms for programmable mechanical structures. *J. Mech. Robot.* **2024**, *16*, 061008. [\[CrossRef\]](#)

49. Hagh, Y.S.; Mohammadi, M.; Mikkola, A.; Handroos, H. An experimental comparative study of adaptive sigma-point Kalman filters: Case study of a rigid-flexible four-bar linkage mechanism and a servo actuator. *Mech. Syst. Signal Process.* **2023**, *191*, 110148. [[CrossRef](#)]
50. Belleri, B.K.; Kerur, S.B. Dynamic analysis of four bar planar mechanism extended to six-bar planar mechanism with variable topology. *Adv. Mech. Des. Mater. Manuf.* **2018**, *1943*, 020094. [[CrossRef](#)]
51. Belleri, B.K.; Goudar, D.M.; Kerur, S.B. Balancing of planar eight –bar mechanism using genetic algorithm. *Trends J. Sci. Res.* **2023**, *1*, 42–52. [[CrossRef](#)]
52. Pira, B.; Cunaku, I. Synthesis of WATT and Stephenson mechanisms six bar mechanism using Burmester Theory. *Int. J. Curr. Eng. Technol.* **2017**, *7*, 25–29.
53. Moşneguţu, E.; Tomozei, C.; Panainte-Lehăduş, M.; Chiţimuş, D.; Irimia, O. Geometric calculation of the influence of an oscillating sieve’s actuation mechanism position on its motion. *Processes* **2022**, *10*, 1760. [[CrossRef](#)]
54. Mosnegutu, E.; Barsan, N.; Panainte-Lehadus, M.; Chitimus, D.; Tomozei, C. Influence of the crank mechanism position in the motion of an oscillating sieve. *J. Eng. Stud. Res.* **2021**, *27*, 36–43. [[CrossRef](#)]
55. Advance Engineering Solutions, WATT Mechanism. Available online: <http://www.aes.nu/1-5softprod.htm> (accessed on 12 April 2024).
56. Advance Engineering Solutions, Roberts Animator. Available online: <http://www.aes.nu/1-5softprod.htm> (accessed on 12 April 2024).
57. Rector, D.M. Linkage Mechanism Designer and Simulator. Available online: <https://blog.ectorsquid.com/?s=Linkage+Mechanism+Designer+and+Simulator> (accessed on 12 April 2024).
58. PTC Mathcad, Mathcad 15. Available online: <https://www.mathcad.com/en> (accessed on 12 April 2024).
59. OriginLab Corporation. OriginPro 2019b, Version 9.6.5.169. Available online: <https://www.originlab.com/> (accessed on 13 April 2024).
60. Kapsalyamov, A.; Hussain, S.; Brown, N.A.T.; Goecke, R.; Hayat, M.; Jamwal, P.K. Synthesis of a six-bar mechanism for generating knee and ankle motion trajectories using deep generative neural network. *Eng. Appl. Artif. Intell.* **2023**, *117*, 105500. [[CrossRef](#)]
61. Plecnik, M.M. The Kinematic Design of Six-Bar Linkages Using Polynomial Homotopy Continuation. Master’s Thesis, University of California, Irvine, CA, USA, 2015; pp. 1–307.
62. Wang, X. The optimization design of six-bar linkage mechanism. *TELKOMNIKA Indones. J. Electr. Eng.* **2013**, *11*, 4091–4098. [[CrossRef](#)]
63. Watwnabe, K.; Funabashi, H. Kinematic analysis of Stepherson six-link mechanisms. *Bul. JSME* **1984**, *27*, 2863–2870. [[CrossRef](#)]

Disclaimer/Publisher’s Note: The statements, opinions and data contained in all publications are solely those of the individual author(s) and contributor(s) and not of MDPI and/or the editor(s). MDPI and/or the editor(s) disclaim responsibility for any injury to people or property resulting from any ideas, methods, instructions or products referred to in the content.